

# DOUBLE CORE EVOLUTION X. THROUGH THE ENVELOPE EJECTION PHASE

Eric L. Sandquist<sup>1</sup>, Ronald E. Taam<sup>1</sup>, Xingming Chen<sup>2</sup>, Peter Bodenheimer<sup>2</sup>, and Andreas Burkert<sup>3</sup>

<sup>1</sup>Department of Physics & Astronomy, Northwestern University, Evanston, IL 60208; erics@apollo.astro.nwu.edu, taam@apollo.astro.nwu.edu

<sup>2</sup>UCO/Lick Observatory, Board of Studies in Astronomy and Astrophysics, University of California, Santa Cruz, CA, 95064; chen@ucolick.org, peter@ucolick.org

<sup>3</sup>Max Planck Institut for Astronomy, Koenigstuhl 17, D-69117 Heidelberg, Germany; burkert@mpia-hd.mpg.de

Received \_\_\_\_\_; accepted \_\_\_\_\_

## ABSTRACT

The evolution of binary systems consisting of an asymptotic giant branch star of mass equal to  $3M_{\odot}$  or  $5M_{\odot}$ , and a main sequence star of mass equal to  $0.4M_{\odot}$  or  $0.6M_{\odot}$  with orbital periods  $\gtrsim 200$  days has been followed from the onset through the late stages of the common envelope phase. Using a nested grid technique, the three-dimensional hydrodynamical simulations of an asymptotic giant branch star with radii  $\sim 1$  A.U. indicate that a significant fraction of the envelope gas is unbound ( $\sim 31\%$  and  $23\%$  for binaries of  $3M_{\odot}$  and  $0.4M_{\odot}$ , and  $5M_{\odot}$  and  $0.6M_{\odot}$  respectively) by the ends of the simulations, and that the efficiency of the mass ejection process  $\sim 40\%$ . During an intermediate phase, a differentially rotating structure resembling a thick disk surrounds the remnant binary briefly before energy input from the orbits of the companion and remnant core drive the mass away. While the original volume of the giant is virtually evacuated in the late stages, most of the envelope gas remains marginally bound on the grid. At the ends of our simulations, when the orbital decay timescale exceeds about 5 years, the giant core and companion orbit one another with a period of  $\sim 1$  day (2.4 days for a binary involving a more evolved giant), although this is an upper limit to the final orbital period. For a binary of  $5M_{\odot}$  and  $0.4M_{\odot}$ , the common envelope may not be completely ejected. The results are not found to be sensitive to the degree to which the initial binary system departs from the synchronous state.

*Subject headings:* binaries: close — circumstellar matter — hydrodynamics — stars: interiors

## 1. Introduction

There are many classes of binary systems which cannot be understood without a phase of significant mass and angular momentum loss. Among those classes are interacting binary systems containing white dwarf or neutron star components. Common envelope evolution has been identified as a means by which the interactions between the two progenitor components lead to the ejection of a large fraction of the mass of the system and to the shrinkage of the binary orbit (see Paczynski 1976). Provided that the common envelope is successfully ejected, a long-period system ( $P \sim \text{years}$ ) can be transformed into a short-period system ( $P \sim \text{days}$ ) consisting of the remnant core of the red giant and its companion.

A binary system can evolve into the common envelope stage whenever the red giant progenitor of the compact component enters a phase where it is not corotating with respect to the orbit at the onset of or during mass transfer to its companion. This may occur when mass transfer from the more massive star to its companion is unstable, as occurs when the Roche lobe contracts faster than its radius, especially in the case of a giant with a deep convective envelope (see Paczynski & Sienkiewicz 1972; Webbink 1979). Another evolutionary path leading to the common envelope stage involves a tidal instability (Darwin 1879; Counselman 1973; Kopal 1978; Lai, Rasio, & Shapiro 1993, 1994), which occurs when a system reaches a minimum value of the total angular momentum for a synchronized close binary system. Evolution to this stage inevitably leads to the infall of one component into its more massive companion.

As a result of the development of powerful numerical algorithms and the advancement of computer technology, progress has been made in modeling common envelope interactions from the slow initial phase to the rapid phase of orbital shrinkage. Many of the simplifying approximations of the past regarding the input physics, as well as the dimensionality of the problem, have been relaxed. In particular, the multidimensional studies of Bodenheimer & Taam (1984), Livio & Soker (1988), and Taam & Bodenheimer (1989) revealed that matter is preferentially ejected at higher than the escape speed along the equatorial plane of the binary system. This theoretical result received observational support from the elliptical or butterfly-shaped appearance of planetary nebulae with binary nuclei (Bond & Livio 1990). That is, the morphology of such nebulae are consistent with the density contrast between the pole and equator seen in common envelope simulations used in interacting winds models (Kwok 1982; Soker & Livio 1989; Frank et al. 1993; Mellema & Frank 1995; Livio 1995). This nonspherical ejection follows from the angular distribution of the energy and angular momentum deposited in the common envelope by the orbital motion of the two components.

Population synthesis calculations by a number of investigators (see, for example, Tutukov and Yungelson 1979; Iben & Tutukov 1984; van den Heuvel 1987; de Kool 1992; Iben & Livio 1993; Yungelson, Tutukov, & Livio 1993; Han, Podsiadlowski, & Eggleton 1995; Kalogera & Webbink 1996; de Kool 1996) have used approximations to the common envelope phase to predict the properties of systems which survive. Such calculations make use of energetic arguments, and the

results are sensitive to the adopted value of the efficiency of the common envelope phase (taken to be equal to the ratio of the binding energy of the ejected mass to the energy lost from the binary orbit). Although the results of the early numerical studies of Taam, Bodenheimer, & Ostriker (1978), Meyer & Meyer-Hofmeister (1979), Delgado (1980), Bodenheimer & Taam (1984), Livio & Soker (1984, 1988), and Taam & Bodenheimer (1989, 1991) were instructive, the important details of the outcome of the common envelope phase were still unclear, since understanding of the mass ejection process was affected by the approximations (such as using smaller numbers of spatial dimensions, or imposed descriptions for the orbital energy dissipation) needed to make the problem tractable. Thus, the production of short-period binary systems containing compact objects remained to be clarified (even if sufficient energy was lost from the orbit to unbind the common envelope) since the results of detailed calculations have not been taken into account in the population synthesis studies in determining whether the two stars would stop spiraling toward each other (see Taam & Bodenheimer 1991).

In this paper, we investigate the details of the hydrodynamics of the common envelope phase in the vicinity of the double core at high spatial resolution in three dimensions in order to understand the termination of the spiral-in phase. Previous three-dimensional studies (de Kool 1987; Terman et al. 1994, 1995; Terman & Taam 1996; Rasio & Livio 1996) have relied on the smoothed particle hydrodynamics technique (SPH; e.g., Lucy 1977; Gingold & Monaghan 1977; Monaghan 1985, 1992). The numerical results of such studies indicated that mass is ejected from the common envelope, although the poor spatial resolution of the simulations made it unclear whether the companion would spiral into the red giant core. Although the SPH technique can model the global features of the evolution during earlier stages, our experience indicates that the numerical resolution is not entirely adequate to model the region of steep density gradients above the red giant core during the terminal phase of evolution. In addition, the large number of time steps required to follow the ejection of a significant fraction of the envelope using higher resolution is computationally prohibitive.

To adequately resolve the region close around the double core, we use a finite differencing numerical technique. In contrast to the study of Livio & Soker (1988), we use an Eulerian nested grid technique similar to that used in Yorke et al. (1995), but extended to three dimensions. We report on the results of simulations of the common envelope phase for binaries consisting of an intermediate-mass asymptotic giant branch star of either 3 or 5  $M_{\odot}$  with a main sequence companion of 0.4 or 0.6  $M_{\odot}$ . In the following section we describe the numerical methods used, the assumptions underlying the calculations, and the construction of the initial models. The detailed evolution of a binary from the initial spiral-in phase through the late phase of envelope ejection is presented in §3, as are comparisons with our other simulations, and a discussion of physics affecting the system beyond the scope of our simulations. The implications of the simulations are discussed in the final section.

## 2. Numerical Methods

For all of the simulations in this paper, a 3-D grid-based hydrodynamics code is used. A nested grid technique is employed to provide higher spatial resolution in the inner regions of the common envelope, with dynamical coupling between grids based on the technique of Berger & Oliger (1984) and Berger & Colella (1989), as described in Yorke, Bodenheimer, & Laughlin (1993) and Ruffert (1993). We have modified a version of the code used by Burkert & Bodenheimer (1993), which they used to follow the isothermal gravitational collapse of a protostar. In our simulations, the main grid has  $64 \times 64 \times 64$  cubical zones, while the nested subgrids have  $64 \times 64 \times 32$  cubical zones, where the short dimension is perpendicular to the orbital plane. Two subgrids were centered within the main grid, and were kept motionless with respect to it. The first subgrid was a factor of 4 smaller in the  $x$  and  $y$  directions, and the second subgrid was a factor of 2 smaller than the first, so that the zone size on the finest grid was  $1.56 \times 10^{11}$  cm in all but one of the simulations (for which it was twice as large). The total mass, energy, and angular momentum of the gas lost from the main grid were followed.

In order to simulate realistic interactions between a giant star and a main sequence companion, the code also follows the motions of two collisionless particles — one for the core of the red giant star, and one for the companion. Gravitational interactions between the collisionless particles and the gas were smoothed in a manner suggested by Ruffert (1993):

$$\Phi_{PG} = \frac{-GM_P}{\sqrt{r^2 + \epsilon^2 \delta^2 \exp(-(r/\epsilon\delta)^2)}},$$

where  $\delta$  is the width of a zone on the innermost subgrid, and  $\epsilon = 1.5$ . Here  $r$  is the distance between the gas and the particle of mass,  $M_P$ . The gravitational potential of the gas was computed separately on the main grid and subgrids via fast Fourier transforms. Boundary values for the subgrid computations were taken from the smallest grid that encompassed it.

Timesteps for each grid were chosen according to a Courant-Friedrichs-Lewy condition on that grid:

$$\Delta t = C\delta_i / \max(|u_x| + |u_y| + |u_z| + c_s),$$

where  $C = 0.5$  is the Courant factor, and  $c_s$  is the sound speed. On the innermost subgrid, the timestep can be reduced to

$$\Delta t = C\delta / \max(|v_1|, |v_2|)$$

if this is smaller than the timestep derived from the gas, where  $v_1$  and  $v_2$  are the speeds of the two collisionless particles. Changes to the Courant number were made as tests, but these had no effect on the results.

Core particles were stepped in position using a four-point Runge-Kutta integration scheme each time the gas distribution was recalculated on the innermost subgrid. When the cores are at their closest approach, the orbits only pass through a handful of zones, so that with the Courant-type timestep, the final orbit would be poorly integrated. To improve on this, the gas

timestep was increasingly subdivided to ensure that the core positions are computed at least 25 times during each orbit.

Because the original version of the code was intended for use in computing isothermal collapse, the code was modified to explicitly treat the internal energy of the gas. The equation of state was chosen to be a combination of ideal gas and radiation pressure (the regions where the gas is affected by electron degeneracy are sufficiently compact that they can be assumed to be restricted to the point masses). Internal energy density was advected in exactly the same manner as mass density, and compressional heating of the gas was also included. Shocks in the gas were handled with an artificial viscosity of the type introduced by von Neumann and Richtmeyer (1950) with a constant shock smoothing length of  $1.18\delta_i$ , where  $\delta_i$  is the zone size in grid or subgrid  $i$ . Advection of density, internal energy, and momentum across zone boundaries was handled with a monotonic transport formalism (van Leer 1977), which provides second-order spatial accuracy, and quasi-second order accuracy in time.

A number of additional tests were conducted in order to check the accuracy of the code for common envelope simulations. First, we conducted a standard shock tube run (Sod 1978), verifying that the numerical results matched the analytical solution for adiabatic flow. The results were substantially similar to those of Burkert & Bodenheimer (1993). We verified that the shocks were not disturbed by the presence or absence of subgrids in the calculation. Secondly, several trial common-envelope runs were conducted to check the accuracy of various aspects of the code. The most important effects involved the smoothing length used in gravitational interactions between core particles and the gas. The value of the smoothing length  $\epsilon\delta$  adopted is a minimum acceptable value — lower values resulted in unacceptable non-conservation of total energy. Because of the importance of understanding the orbital evolution of the core particles after the majority of the gas has been forced away during the infall of the companion, the smoothing length was reduced as much as possible. The same gravitational smoothing length was used in all levels of each simulation since it was found that significant non-conservation of total energy occurred if the point mass came near the edge of a subgrid during simulations in which the smoothing length was made equal to  $\epsilon$  times the size of a zone in the grid which the particle was situated.

The degree of physical precision of our calculations depends on the resolution of the gas in the regions of strongest interaction (the number of subgrids used) and on the accuracy of the force calculation near the core particles (the core-gas smoothing length). The degree to which energy was conserved depended on the maximum strength of the core gravitational fields (which was determined by the smoothing length). A similar effect was found by Ruffert (1993), in that the density and temperature structure near the core was sensitive to the structure of the core potentials. After a number of tests, it was found that for a given smoothing length, fewer subgrids resulted in slightly better conservation of energy. This motivated our use of only two subgrids. We will return to this topic in § 3.5, where we discuss the effects of resolution on the final orbital separation.

## 2.1. Initial Models

The initial gas distribution in the envelope of the red giant was derived from one-dimensional stellar models obtained from the code developed by Eggleton (1971, 1972). Interpolation within a stellar model in the appropriate evolutionary state was used to obtain densities and internal energies for the zones. A diffuse background gas filled the remainder of the grid, and was given a temperature to bring it into pressure equilibrium with the surface of the star. The mass of the core particle for the giant was chosen to bring the total giant mass to that of the input stellar model. The orbit of the binary was placed in the  $xy$ -plane. We also forced the gas to be symmetric about this plane, so that at all times the core particles remained very close to  $z=0$ .

In order to determine the sensitivities of the outcome of the common envelope evolution, we have varied three parameters: the companion mass, the red giant mass, and the fraction of synchronous rotation given to the envelope of the giant. Our baseline simulation, against which we will compare all of our runs, involved a  $3M_{\odot}$  red giant star (with a  $0.7M_{\odot}$  core, and a total radius of  $1.39 \times 10^{13}$  cm), and a  $0.4M_{\odot}$  companion particle. The companion was initially placed in a circular orbit at a distance of  $2 \times 10^{13}$  cm, with the giant in synchronous rotation with the companion. For the other simulations, these parameters were varied, and the alternate values used were: a  $0.6M_{\odot}$  companion; a  $5M_{\odot}$  giant star (with the same radius as the  $3M_{\odot}$  giant, but with a  $1M_{\odot}$  core); and a non-rotating giant. One additional simulation involving a more evolved  $5M_{\odot}$  giant with a radius of  $2.46 \times 10^{13}$  cm was run with a companion of  $0.6M_{\odot}$  orbiting at a distance of  $3.7 \times 10^{13}$  cm.

We have not started our baseline simulation in a relaxed-binary configuration as did Rasio & Livio (1996), but we believe that the difference in the initial conditions is a minor consideration. In the Rasio & Livio’s (1996) case, matter was barely overflowing the giant’s Roche lobe whereas in our initial configuration the mass transfer developed quickly. This difference in initial conditions results in a sharper angle of impact for the companion star onto the giant’s surface in our simulation. In addition, the efficiency of mass ejection from the binary system is somewhat underestimated in the present study since the energy transfer from the orbit to the giant envelope to bring it to a Roche-lobe filling configuration is already incorporated into the envelope in the initial state described by Rasio & Livio (1996). However, this difference is not important for the final outcome since this aspect of the evolution affects only the near-surface gas, which is the least bound material. Hence, the energy difference is rather small in that sense. Most importantly, the general agreement in the final state of our simulations between the synchronously rotating and asynchronously rotating cases argues that the effects of the initial conditions are minor. In particular, the evolution and timescales for the rapid dynamical phase and mass ejection phase are unaffected by these details of the initial configuration.

### 3. Results

In this section we report on the numerical results of five simulations. The initial parameters and results for each sequence are summarized in Tables 1 and 2 respectively. For convenience, the results are presented in detail for the baseline simulation (sequence 1) followed by descriptions of the differences that exist among the simulations. For sequence 1, we consider the common envelope evolution of a binary consisting of a  $3M_{\odot}$  asymptotic giant branch (AGB) star with a  $0.4M_{\odot}$  main sequence companion. The two components are orbiting about their common center of mass in circular motion with a period of 1.2 years.

#### 3.1. Spiral-In Phase

In the earliest phase of the evolution, gas from the near surface of the giant star is gravitationally torqued up, removing energy and angular momentum from the binary orbit in the process. (The energy and angular momentum as a function of time are shown in Figures 1 and 2.) We define this initial phase as the time interval between the beginning of the simulation (a state approximating a realistic initial binary orbit) and the time at which the separation of the point masses is equal to the initial radius of the giant. In our baseline simulation, this phase lasts 160 days.

During this initial phase, there is a period of fairly heavy mass transfer from the giant to the companion. The matter stream is dragged around behind the companion’s direction of travel into an orbit until the stream impacts itself, after which it quickly fills the companion’s potential well.

By the time the companion reaches the former surface of the giant, the core and companion have transferred about one-third of their angular momentum to the gas. Very little mass has been unbound at this point though, and none has been lost. In addition, the energies in the system have changed very little, as the gas surrounding the giant core (which contains most of the energy) has not been significantly affected by the distant influence of the companion.

#### 3.2. Rapid Infall Phase

Once the companion has entered the envelope, which is still mostly intact, the orbital decay rate of the binary ( $-\dot{a}$ ) has almost reached its maximum value (over a percent of the giant’s radius per day; see Figures 3 and 4). Over the course of the next 100 days the majority of the change in the core-companion separation occurs. We define the end of this phase as the time at which the orbital decay timescale begins increasing again, after holding at a roughly constant value. This occurs after approximately 400 days. In this simulation, about 90% of the remaining orbital angular momentum is transferred to the gas, mostly during the early part of the phase when the binary separation is decreasing most rapidly.

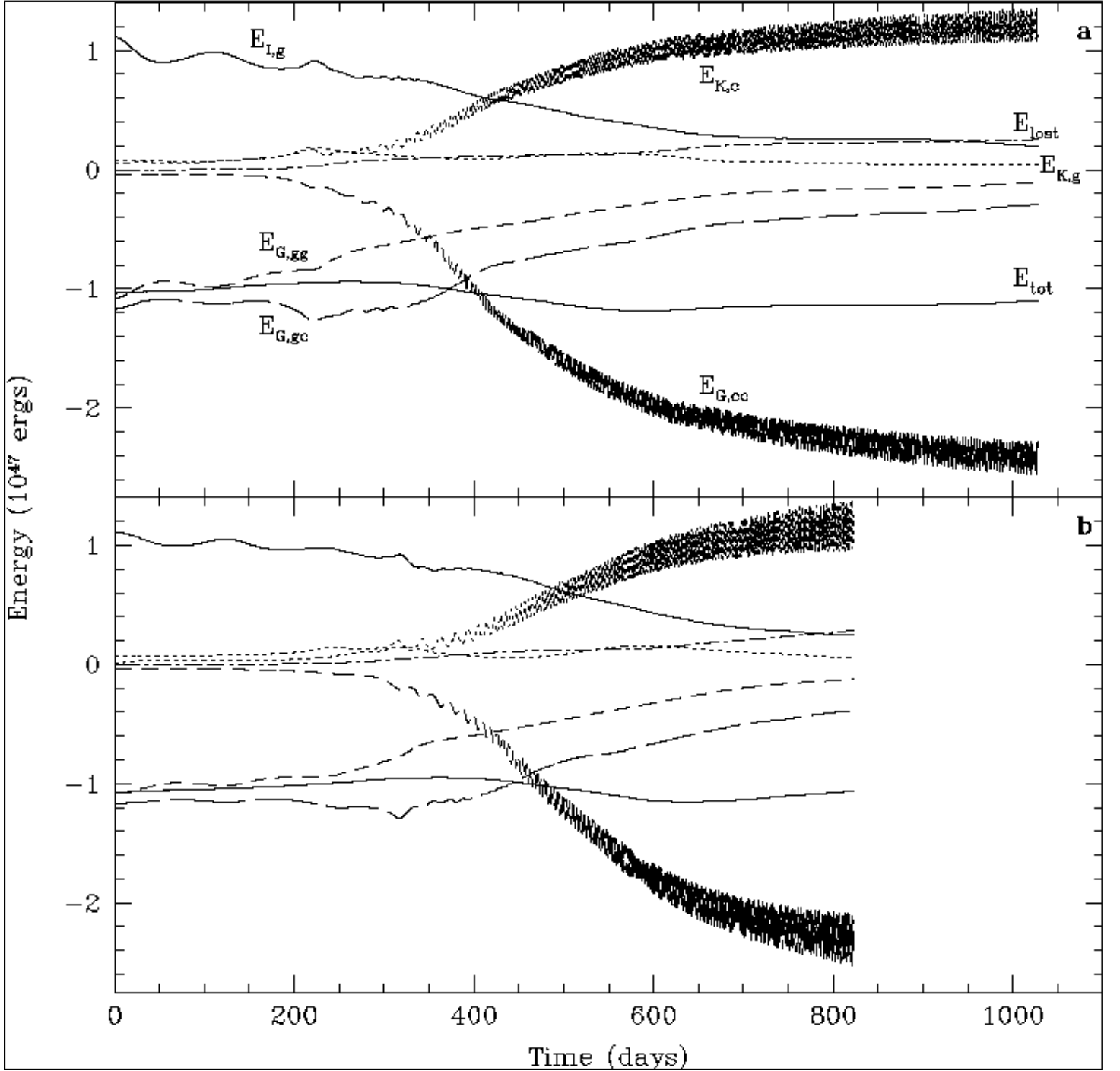


Fig. 1.— The contributions to the energy for a) simulation 1 and b) simulation 2 (no initial rotation of the gas). The curves from top to bottom at 700 days are: kinetic energy of the point masses ( $E_{K,c}$ ), internal energy of the gas ( $E_{I,g}$ ), energy lost from the grid ( $E_{lost}$ ), kinetic energy of the gas ( $E_{K,g}$ ), potential energy from gas-gas interactions ( $E_{G,gg}$ ), and from gas-point mass interactions ( $E_{G,gc}$ ), total energy, and potential energy from core-companion (point mass) interactions ( $E_{G,cc}$ ).



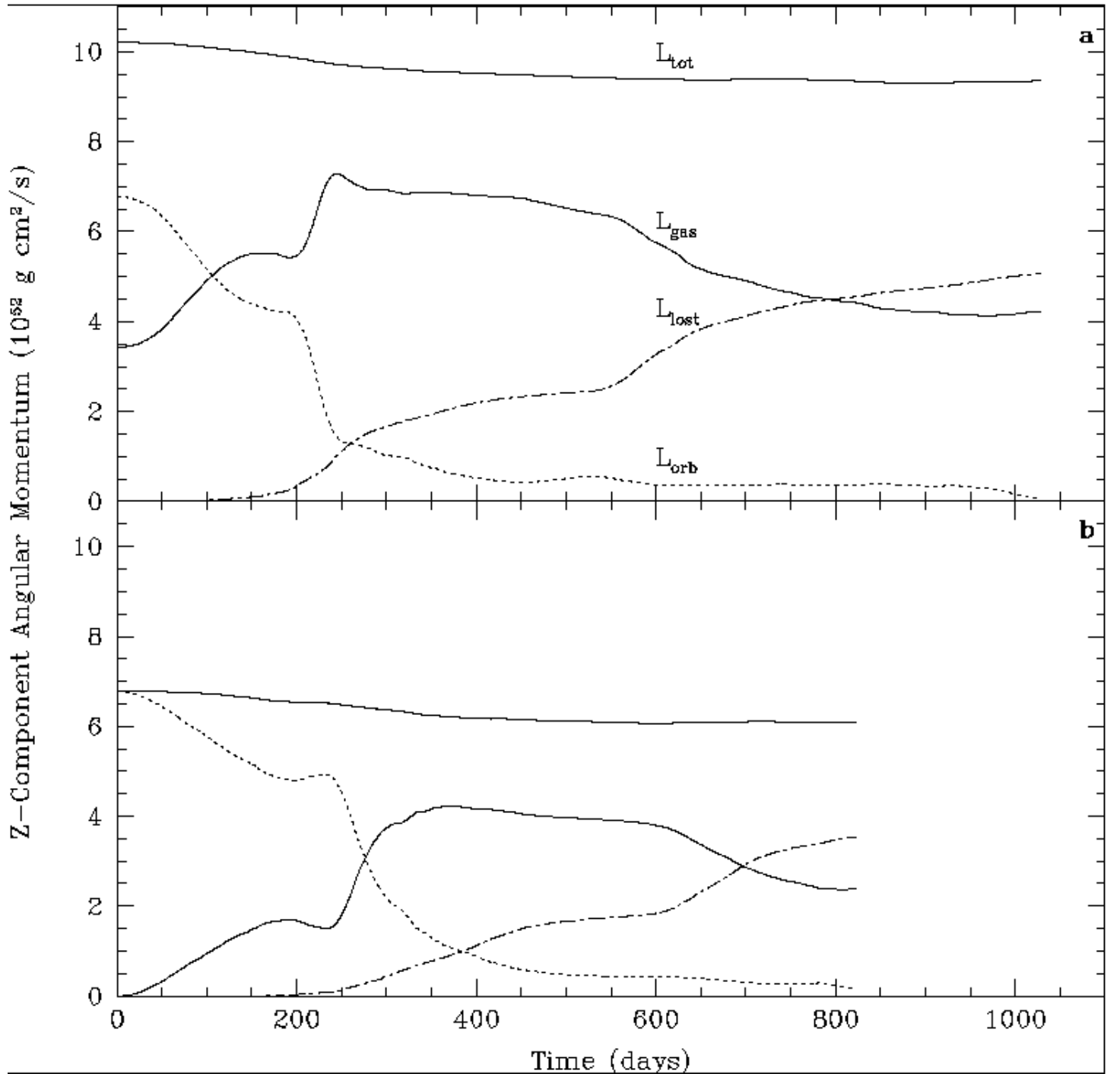


Fig. 2.— The contributions to the z-component of the angular momentum for a) simulation 1 and b) simulation 2 (no initial rotation of the gas). The curves from top to bottom at 600 days are: total, gas, lost from the grid, and orbital (carried by the point masses) angular momentum.

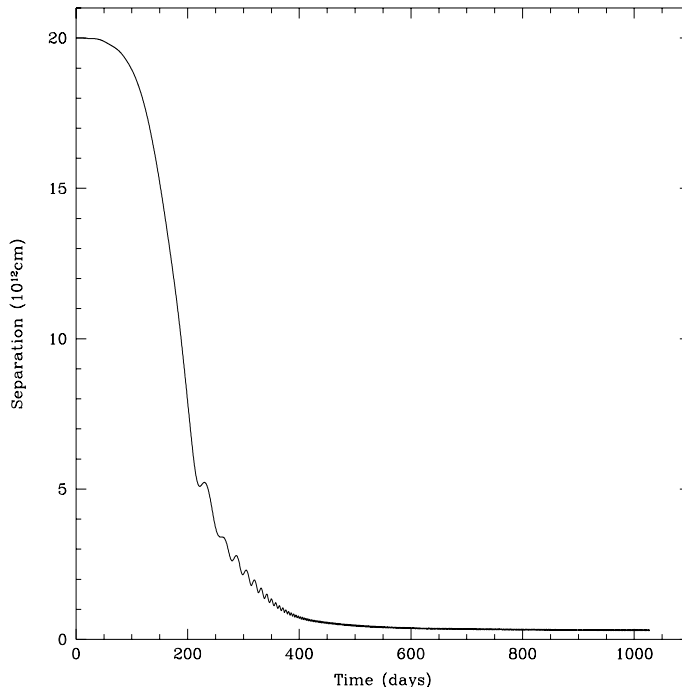


Fig. 3.— The orbital separation between the two point masses in simulation 1.

In the early portions of this stage, when the core-companion separation is decreasing most quickly (on a timescale of about 100 days), the gas flowing past the companion is accelerated to supersonic velocity. A bow shock is generated in this gas flow, directed more or less in the direction of travel of the companion, as is visible in the entropy contour plots in panel a of Figure 5. Later on when the point masses have spiralled closer, weak spiral shock waves can be seen in the density contours (see Figure 6). At first, only one shock is generated — in front of the more rapidly moving companion. As a result, mass is pushed away from the giant in a very asymmetric pattern. Even later, shock waves are generated in front of both point masses. Near the point masses (before the waves have gone through one-quarter of a turn), the shock waves are strongest, in the sense that more entropy is generated in the gas. When the shock waves finally propagate into regions of lower density, the Mach number of the gas increases, and they become more visible in the entropy plots (as in panel b of Figure 5). These shock waves are the primary means for transporting angular momentum away from the point masses during this phase.

Spiral shock waves continue to move outward from the point masses throughout this phase. Because the period of the binary orbit is considerably smaller than the orbital timescale of the envelope gas, the spiral waves become tightly wound. The angular momentum input from the shocks causes the mass distribution to elongate in the  $xz$ -plane, as seen in panel c of Figure 7. The peak energy transfer occurs shortly after this point as the companion begins to dissipate energy in the high density gas at the core of the giant. At the same time, the angular momentum transfer from the point mass orbits to the gas is shutting off. The gas near the two cores is torqued up, but

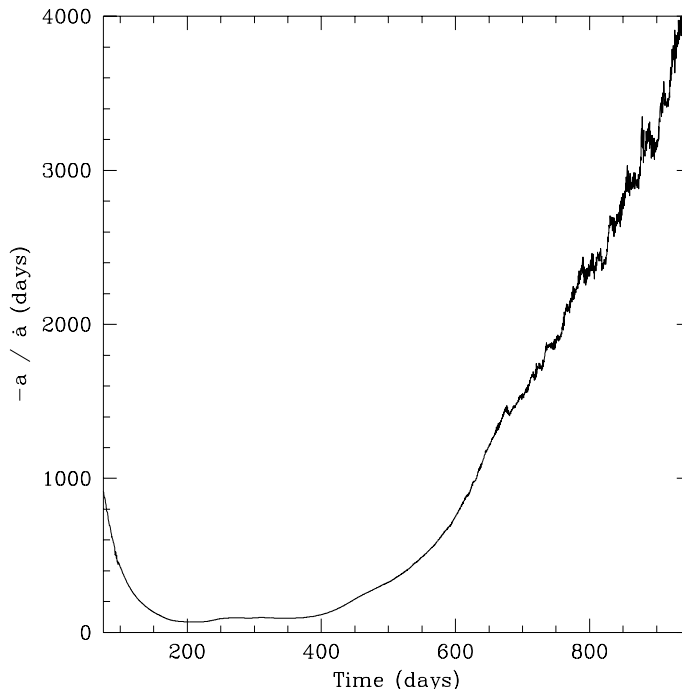


Fig. 4.— The orbital decay timescale ( $-a/\dot{a}$ ) for the point masses in simulation 1. A time-averaged orbital separation has been used in computing the timescale.

only a very small region ( $\approx 10^{12}$  cm in diameter) following the companion’s spiral wave reaches angular velocities near corotation. At the very end of the phase, the spiral shocks are very weak everywhere except in the vicinity of the point masses. Outside this region, the gas motions are close to radial, which is the direction normal to the spiral waves. A thick disk-like structure begins to take shape towards the end, and a low density region forms along the rotation axis (see panel d of Figure 7).

The peak energy transfer from the orbits of the companion and the core to the gas occurs when the two particles are deep in the potential well of the system where more energy is available per unit change in separation. Very little of this energy has been converted into kinetic energy of the gas though. From Figure 8, we infer that most of the energy lost from the orbit is used in powering a relatively slow expansion of the mass closest to the core and companion. At the end of the phase there is little mass ( $< 0.03 M_{\odot}$ ) within a distance of several times the orbital separation from the point masses — more than half of the original content has been pushed outwards. On the other hand, the amount of mass within the original radius of the star has decreased by about 30%. This trend continues into the next phase of the evolution.

Through the midpoint of this phase, the specific entropy profile increases monotonically with cylindrical radius (see Figure 9). By the end of the phase, a small amount of mass ( $\approx 0.1 M_{\odot}$ ) near the core has developed a profile that decreases outward, which indicates convective instability.

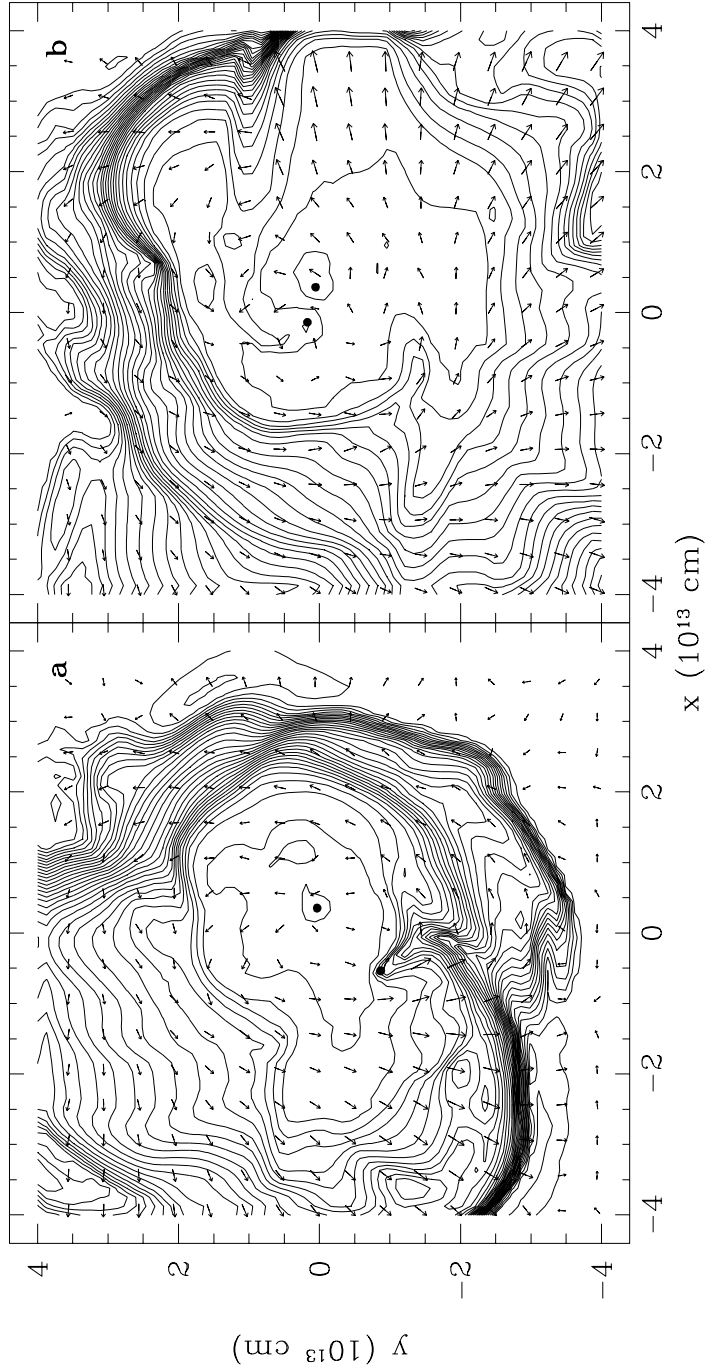


Fig. 5.— Specific entropy contour plots at a) 170 days and b) 234 days. Entropy contours are at intervals of 0.01 in the logarithm. Solid dots indicate the positions of the point masses.

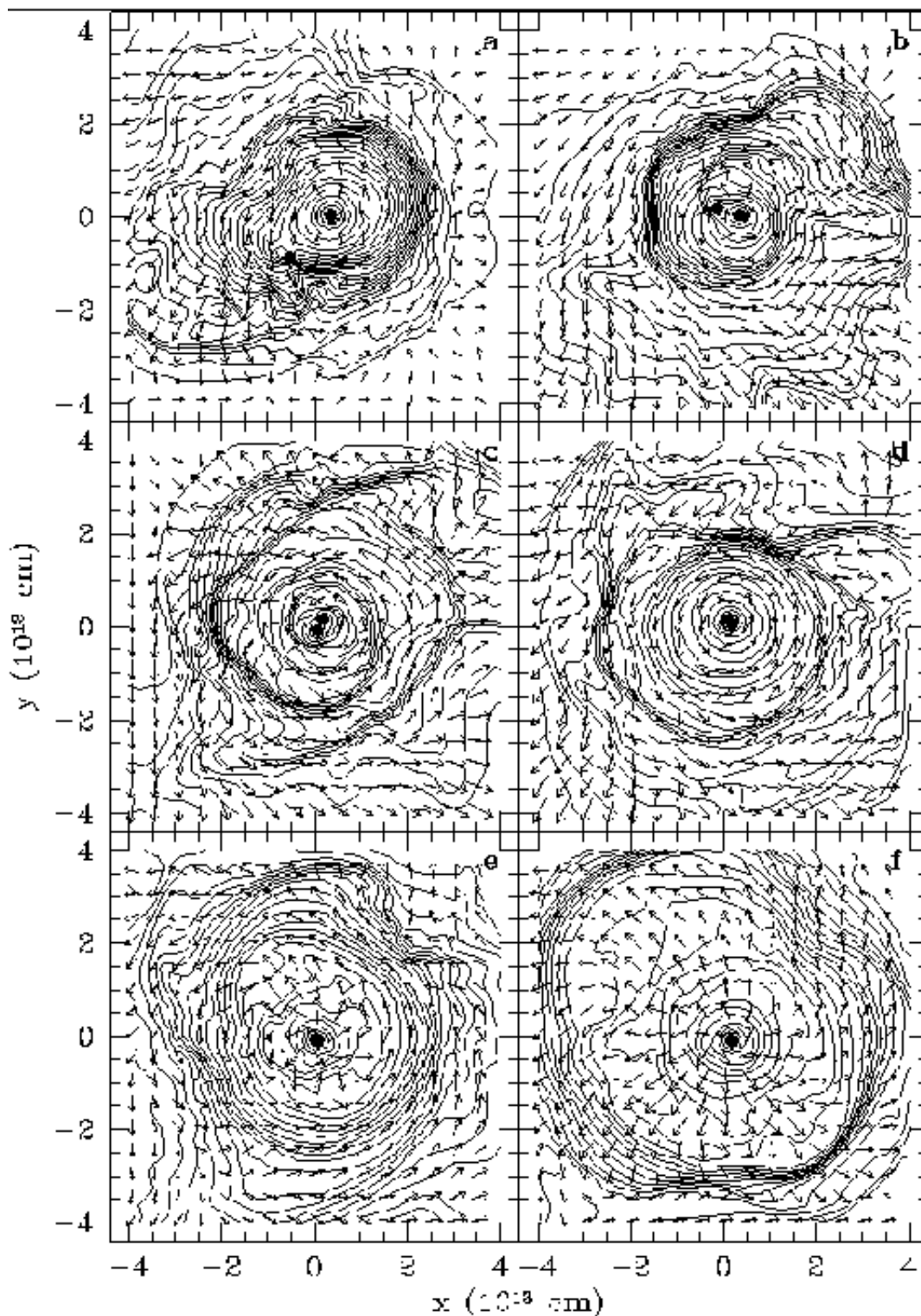


Fig. 6.— A sequence of density contour plots in the orbital plane during simulation 1. Contours are five per decade in density. Solid dots indicate the positions of the two point masses. The velocity vector field is scaled to the maximum value in each frame. From left to right, and top to bottom, the age of the simulation at the time of snapshots is a) 170 days, b) 234 days, c) 289 days, d) 372 days, e) 462 days, and f) 530 days.

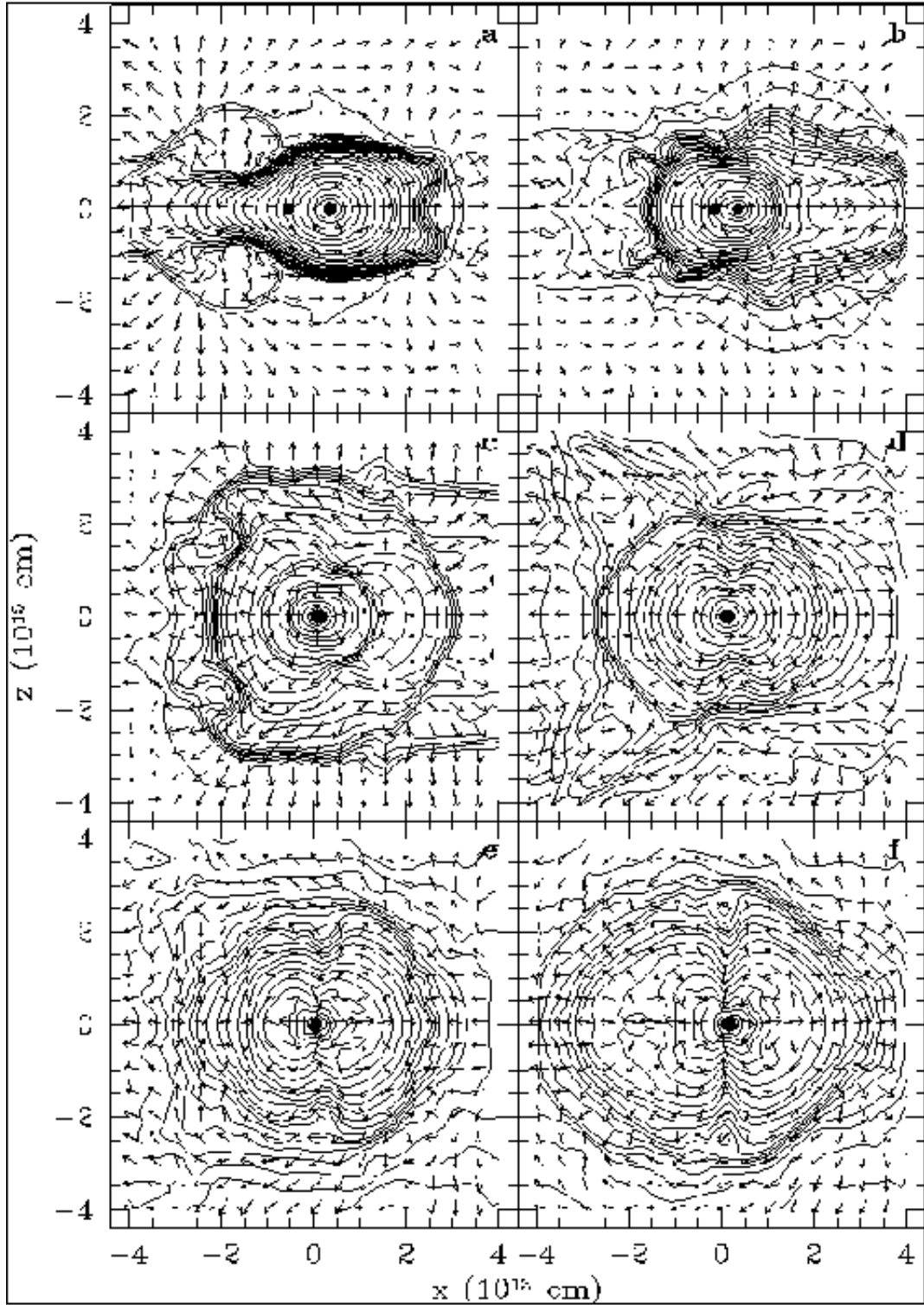


Fig. 7.— A sequence of density contour plots perpendicular to the orbital plane during simulation 1. The legend is the same as in Figure 6.

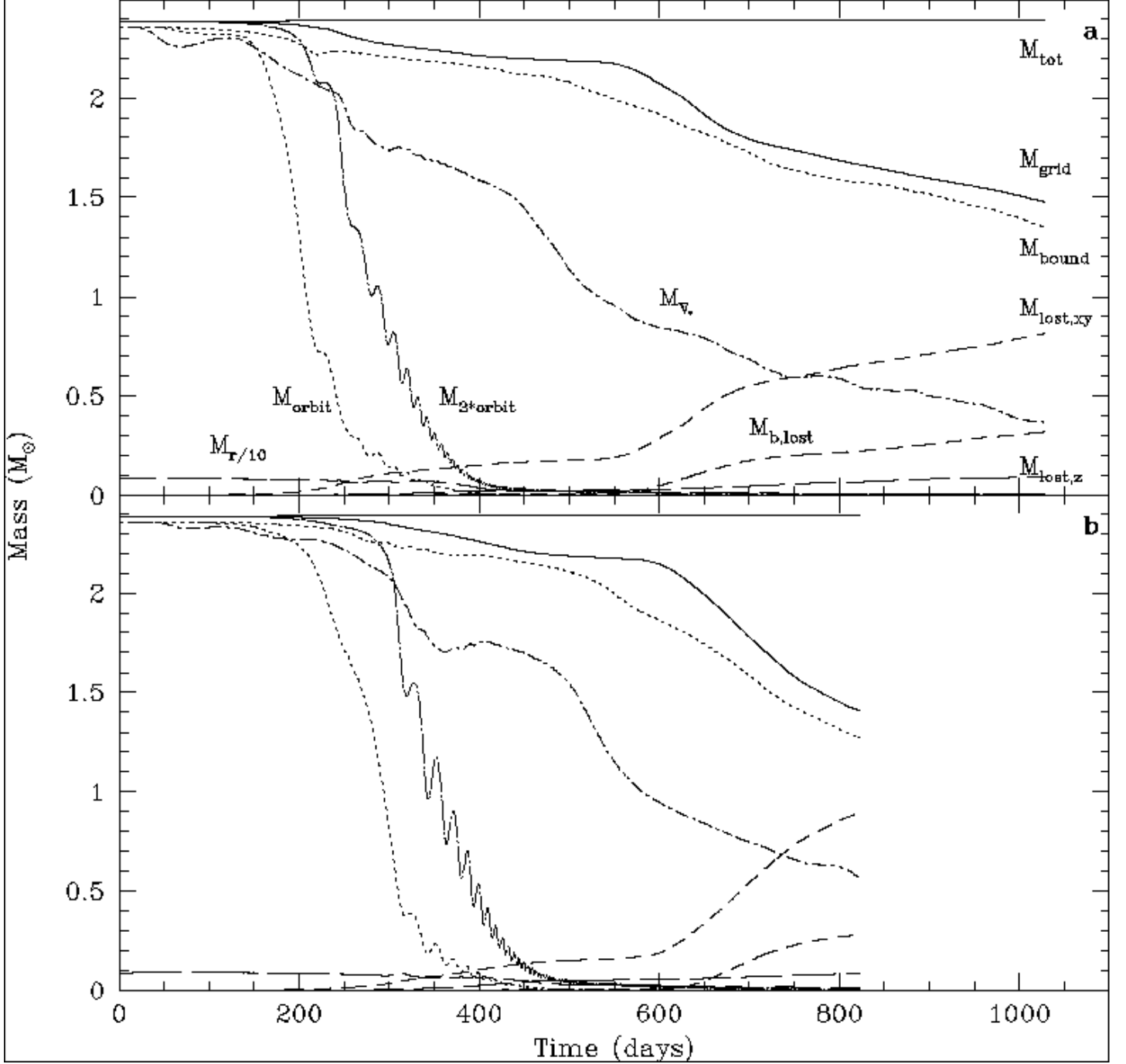


Fig. 8.— Tracers of gas mass for a) simulation 1 and b) simulation 2 (no initial rotation of the gas). The curve labels are as follows:  $M_{tot}$ , total mass;  $M_{grid}$ , mass remaining on the grid;  $M_{bound}$ , mass on the grid that remains bound;  $M_{V_*}$ , mass in the original volume of the giant;  $M_{r/10}$ , mass within a distance of one-tenth the original stellar radius from the core of the giant;  $M_{orbit}$ , mass within a circular orbit the size of the current separation of the point masses;  $M_{3*orbit}$ , same as  $M_{orbit}$ , but with three times the orbital separation;  $M_{lost,xy}$ ,  $M_{lost,z}$ , mass lost from the grid in the radial direction and in the z-direction; and  $M_{b,lost}$ , bound mass lost from the grid.

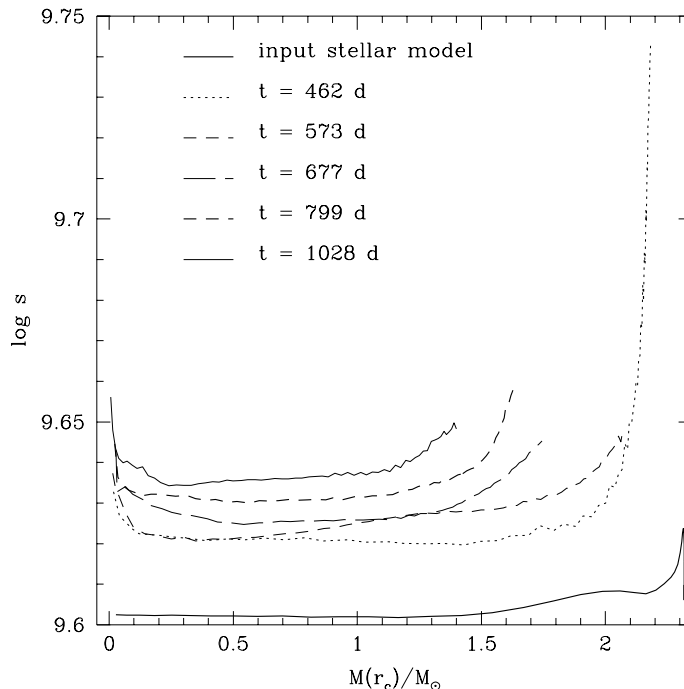


Fig. 9.— Specific entropy profiles as a function of mass within cylindrical shells at various times during simulation 1. The cylindrical radius  $r_c$  is measured from the center of mass of the two point masses.

This region is maintained during the remainder of the simulation, as gas motions apparently do not have time to redistribute the entropy. (In the next phase of the evolution, we do see some evidence of slightly higher entropy blobs in the vicinity of the point masses. This seems to indicate the presence of convection, although the motions of these blobs tend to keep them fairly close to the orbital plane.) At this point, we also find the first indications of circulation perpendicular to the orbital plane with timescales on the order of a year. This entropy profile around the point masses comes into being only when they take up close orbits around each other, and are able to repeatedly shock the gas. At about the same time, the specific angular momentum of gas in the vicinity of the point masses also drops by a large amount (see Figure 10), while much of the gas outside this region gains significantly. This appears to be the result of the flattening of the giant.

At the end of this phase, the point masses are in close, relatively stable orbits about each other. The center of mass of the orbiting point masses has received most of its “kick” from the ejected material also — a speed amounting to just  $3 \text{ km s}^{-1}$ . The cores begin oscillating around the system’s center of mass due to an asymmetry in the gas distribution, probably resulting from the spiral outflow pattern. The majority of the gas is still found within the original volume of the giant, but it continues to flow outwards as a result of the energy input from the core and companion. The energy transfer rate (shown in Figure 11), which reached a peak value of  $1.3 \times 10^6 L_\odot$ , has declined by about half. Further expansion of the gas is facilitated through the



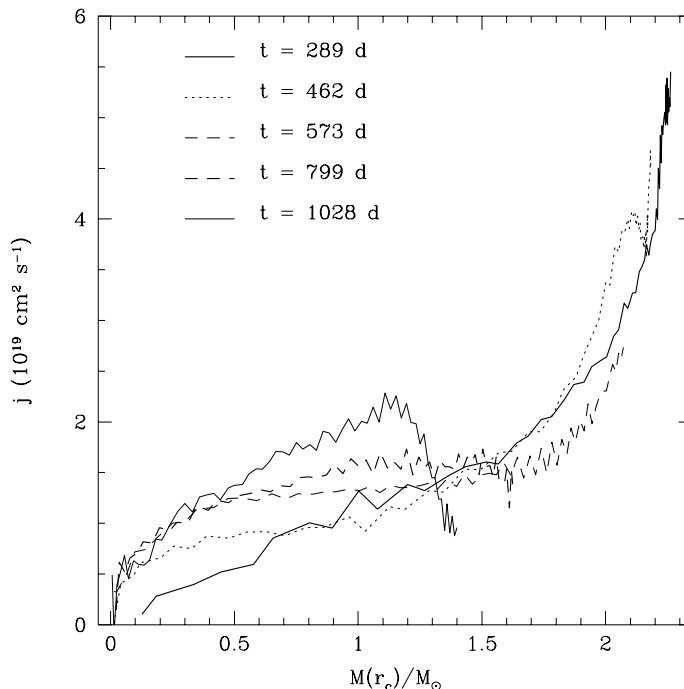


Fig. 10.— Specific angular momentum profiles as a function of mass within cylindrical shells at various times during simulation 1. The cylindrical radius  $r_c$  is measured from the center of mass of the two point masses. The profile for an age of 677 days was not plotted due to its similarity to that for 799 days.

use of a larger proportion of energy taken from the internal energy of the gas. The removal of mass from the vicinity of the point masses was initially driven by spiral shocks, but at the end of this phase the reduced mass near the cores has considerably reduced the efficiency of angular momentum transport by them. Regardless, the gas is distributed primarily in the orbital plane of the binary as a result of the earlier action of these waves.

### 3.3. Envelope Ejection Phase

At the beginning of this phase, the cores have completed the majority of the orbital decay with the separation reaching  $\sim 5 \times 10^{11}$  cm. The orbital decay timescale increases dramatically beyond this point. This is primarily because the mass in the immediate vicinity of the two cores has declined to  $0.025M_\odot$ . There was originally about  $0.1M_\odot$  of gas in this region of the red giant initially — amounts this small are typical of the mass-radius profiles of red giants (see, for example, Figure 6 of Yorke et al. 1995, as well as Figure 12). We note, however, most of the mass loss from the original volume of the giant (which we will call the “ejection”) does not occur until after the cores have established themselves in close orbits about each other.

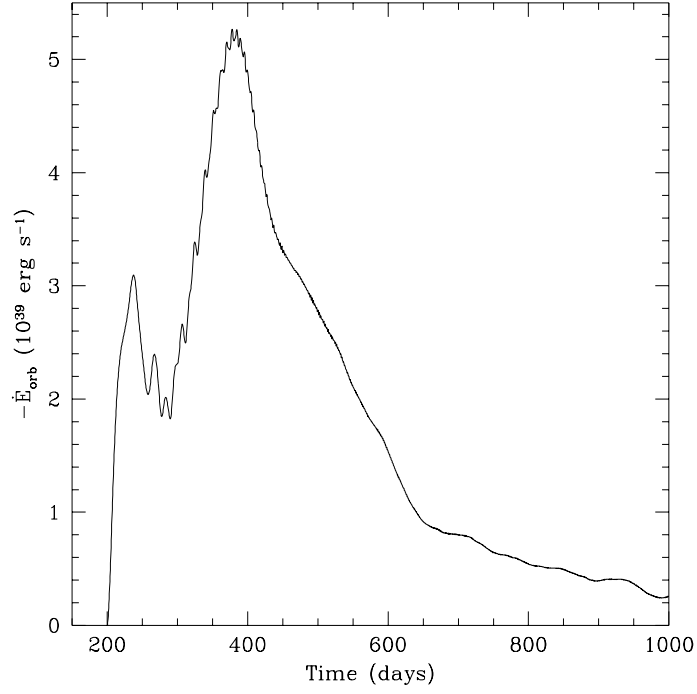


Fig. 11.— The energy dissipation rate from the point masses orbits in simulation 1.

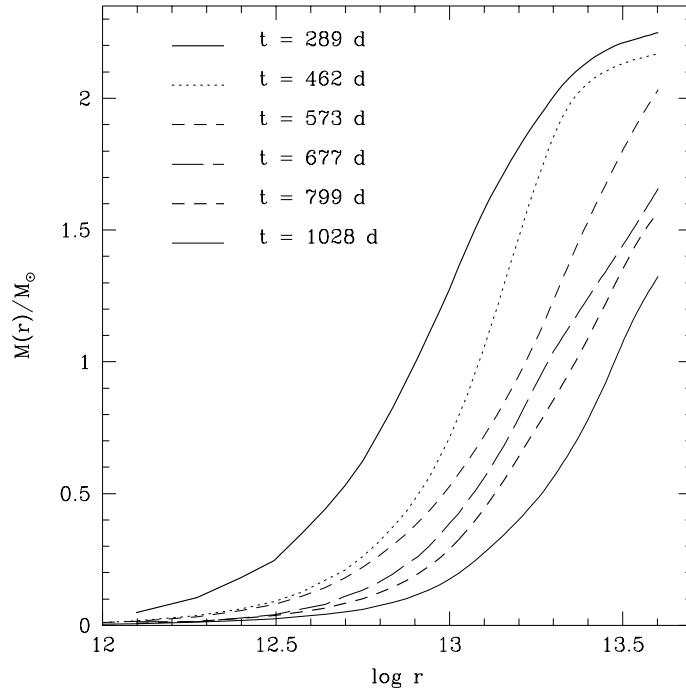


Fig. 12.— Mass-radius profiles for various times during simulation 1. The radius is measured from the position of red giant core.

The gas heated by close interaction with the two cores begins expanding away, and continues expanding through the remainder of the simulation, as shown in panels e and f of Figure 6. The rotational pattern associated with the disk-like structure seen in panel d is quickly overwhelmed by the outflow. The expansion of the gas is driven by continued energy input from the point mass orbits, and is responsible for the movement of most of the remainder of the giant’s mass out of the star’s original volume. This energy input also appears to be the cause of the circulations that develop perpendicular to the plane of the orbit within about  $10^{13}$  cm of the point masses (see especially panels e and f of Figure 7), confirming earlier work by Taam & Bodenheimer (1991) in two dimensions and Terman & Taam (1996) and Rasio & Livio (1996) in three dimensions. The majority of the gas on the grid is still to be found within about one giant radius of the orbital plane.

By 530 days (panel f in the density plots), two thin cones having strong inflow are set up along the rotation axis. These inflows complete the circulation pattern, partially replenishing the gas surrounding the point masses that is being driven out. The strongest outflow is to be found close to the orbital plane, where gas can be accelerated to faster than the local sound speed. From Figure 8 it is apparent that there is a net outflow, as can also be gathered by the fact that the strongest inflow involves relatively low density gas along the rotation axis. At later times, the outflow becomes more confined to the orbital plane ( $\pm 5 \times 10^{12}$  cm).

At the end of the simulation, over 90% of the gas was pushed out of its original volume, and mass was still being removed from the volume at a rate of approximately  $0.3 M_{\odot} \text{ yr}^{-1}$ . About 45% of the gas had been pushed off the edge of the grid, although almost all of what remains is still bound (although marginally) to the system. At the end of the simulation, a significant amount of bound mass had been lost off the grid as a result of the expansion of the gas, making continued calculations unreliable. As was found at the end of the rapid infall phase, the majority of the gas does not have angular velocity more than 10% of corotation. As seen in Figure 13, a small amount of mass is maintained close to corotation very near the orbiting point masses, but the angular momentum transfer is negligible.

In the end, the point masses have a separation of  $4.42R_{\odot}$ . At late times, the fractional decrease in the orbital separation of the cores should equal the fractional decrease in their gravitational potential energy since there is little envelope mass within the binary orbit. We do find that the energy loss and orbital decay timescales go in lockstep. By the end of the simulation, the orbital decay timescale had increased to about 12 years. The mass loss rate for the system (computed from the amount of bound gas) has remained roughly constant over most of the simulation, meaning the mass loss timescale has decreased to about 6 years by the end of the simulation. A comparison of the timescales indicates that the entire common envelope should be ejected. As can be seen from Figure 8, the gas near the two cores is cleared out within about 100 days after the end of the rapid infall phase, and at the end of the simulation only about  $0.37M_{\odot}$  remains in the original volume of the giant.

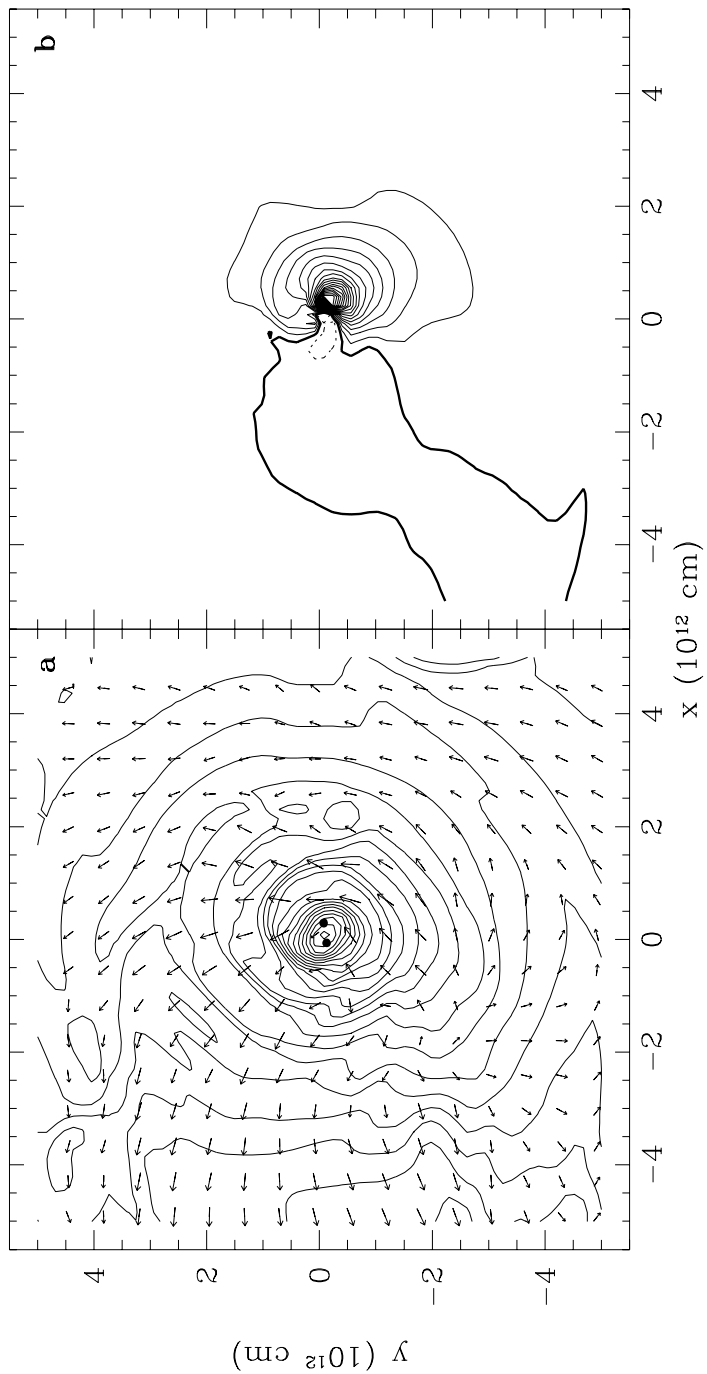


Fig. 13.— Density (panel a) and angular velocity (panel b) contours in the orbital plane for the innermost subgrid at 677 days. Density contours are 5 per decade. Angular velocity contours are at intervals of 2.5% of corotation. The dark solid line indicates the zero rotation contour. The positions of the point masses are indicated in on the density contour plot.

### 3.4. Comparison Simulations

In all but the last of the following sequences, the companion was started on a circular orbit at a distance of  $2.0 \times 10^{13}$  cm away from the core of the giant. In all of the sequences but 2 and 5, the envelope of the giant star was in synchronous rotation with the companion’s orbit. In Table 2, we summarize various characteristics of the system at the end of the simulation: final separation of the point masses, their orbital period, the recoil velocity for the center of mass of the point masses, and the efficiency of envelope ejection  $\alpha_{CE}$ . [We choose to use the definition

$$\alpha_{CE} = \frac{\Delta E_{bind}}{\Delta E_{orb}}$$

(Tutukov & Yungelson 1979), where  $\Delta E_{orb}$  is the change in orbital energy of the point masses (which is the difference in the sum of kinetic plus potential energies — in the final state this was computed for the two point masses, but for the initial state, this was computed using the masses of the companion point mass and the giant), and  $\Delta E_{bind}$  is the binding energy of the mass ejected, as determined from the initial giant model. The mass ejected was taken to be the mass lost from the main grid plus unbound mass remaining on the grid minus bound mass lost from the main grid.] Many details of the sequences are similar, so we will concentrate on the differences in the final orbital parameters and the mass-loss evolution.

#### 3.4.1. Sequence 2: $3 M_{\odot}$ Giant, $0.4 M_{\odot}$ Companion, Nonsynchronous Rotation

In this simulation, the initial conditions were chosen to be identical to those of the baseline simulation, except that the giant envelope was not rotating. The expectation was that the larger relative velocity between the companion and the envelope of the giant would result in a greater deposition of the companion’s orbital energy and angular momentum in the envelope.

A comparison of the mass tracers for the sequences (Figure 8) indicates that the timescale for the companion to enter the envelope of the giant is actually slightly longer for the nonsynchronous case. This is a result of less efficient angular momentum transfer for the nonsynchronous case — in order to begin to enter the envelope, the companion’s orbit must develop eccentricity, as can be seen in Rasio & Livio’s (1996) calculation, and in ours. In this simulation, the companion’s gravitational torque acts for smaller amounts of time on any particular element of the surface of the giant’s envelope.

Mass is removed from the star’s volume and from the grid at approximately the same rate for both simulation 1 and 2. We do not find any observable characteristics of the simulation that would allow us to determine whether the giant in such a binary was out of synchronism at the beginning of the interaction.

### 3.4.2. Sequence 3: $5 M_{\odot}$ Giant, $0.4 M_{\odot}$ Companion

A simulation was run with a  $5M_{\odot}$  AGB star to gauge the effects of different giant star mass (with a more massive core and a more massive envelope) on the evolution. Since the  $5M_{\odot}$  giant had nearly the same initial radius as the  $3M_{\odot}$  giant and the initial orbital separation was the same as in sequence 1, the giant overfilled its Roche lobe by a smaller margin. This sequence was not followed as long as the baseline simulation (891 days, as opposed to 1027 days for sequence 1), but at the end of the simulation the core-companion separation was found to be converging to approximately the same value.

Although the binding energy of the envelope is larger, gas is lost from the original volume of the star and from the grid at nearly the same rate as in the baseline simulation, as shown in Figure 14. The implications are that the energy released from the orbit in these two simulations goes towards almost completely clearing out the region around the orbiting point masses, with the remainder (probably the majority) going toward expansion of the envelope in the orbital plane. If, as appears to be the case, the orbital decay of the point masses is physically slowing (as opposed to slowing due to numerical effects), we would expect that the envelope of the giant would not be completely ejected. At the end of this simulation the orbital decay timescale is about 4 years, which is roughly half what it was at the comparable point in simulation 1. In addition, the orbital decay timescale is increasing at roughly half the rate it was in simulation 1. The mass-loss timescale at the end of the simulation is much longer ( $\approx 27$  years) than the orbital decay timescale, further suggesting that the envelope of the giant might remain close enough to the point masses to affect their orbits further.

The inability of the companion to eject the more massive envelope is also reflected in the efficiency factor  $\alpha_{CE}$  — for this simulation we find that is only 24%, compared to  $\approx 40\%$  for sequences 1, 2, and 4. However, as discussed in § 3.5, a different algorithm for the smoothing length in the gravitational potential leads to considerably more mass ejection and a higher efficiency factor, so these results for this simulation should be treated with care.

### 3.4.3. Sequence 4: $5 M_{\odot}$ Giant, $0.6 M_{\odot}$ Companion

In this simulation, we again find that the companion’s orbital decay has stopped at approximately the same distance from the giant core as it did in the baseline simulation. The flat portion of the initial mass-radius profile of the  $5M_{\odot}$  giant had very nearly the same spatial extent as that of the  $3M_{\odot}$  model, which may explain the similarity if indeed the orbital decay decelerates when the two point masses begin orbiting within this region.

At the end of the simulation (which lasts 742 days), the orbital decay timescale has almost reached 6 years, indicating that the mass near the point masses has been efficiently removed. The timescale is actually increasing faster than in simulation 1. In examining the mass tracers,

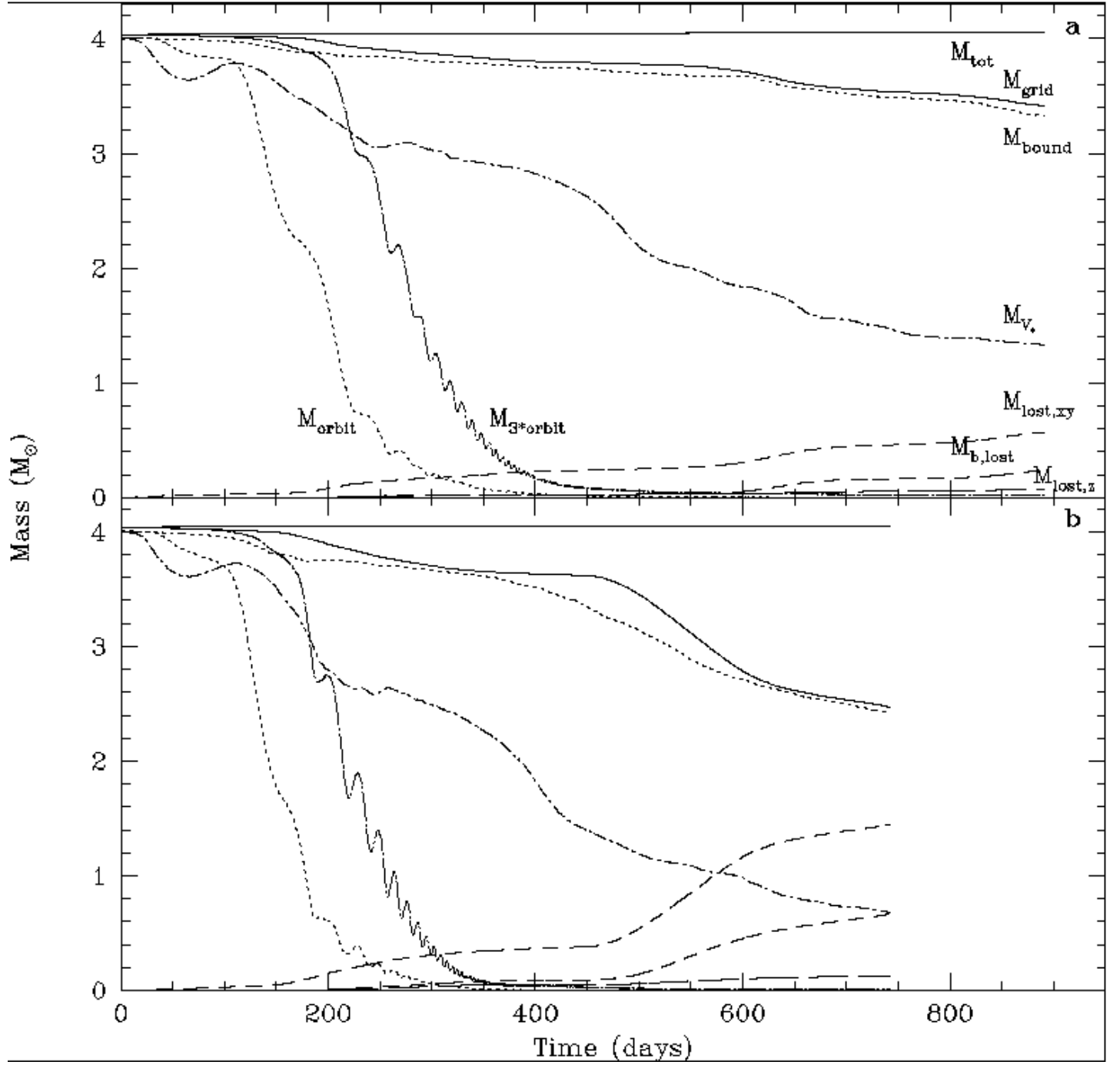


Fig. 14.— Tracers of gas mass for a) simulation 3 and b) simulation 4. The curve labels are the same as found in Figure 8.

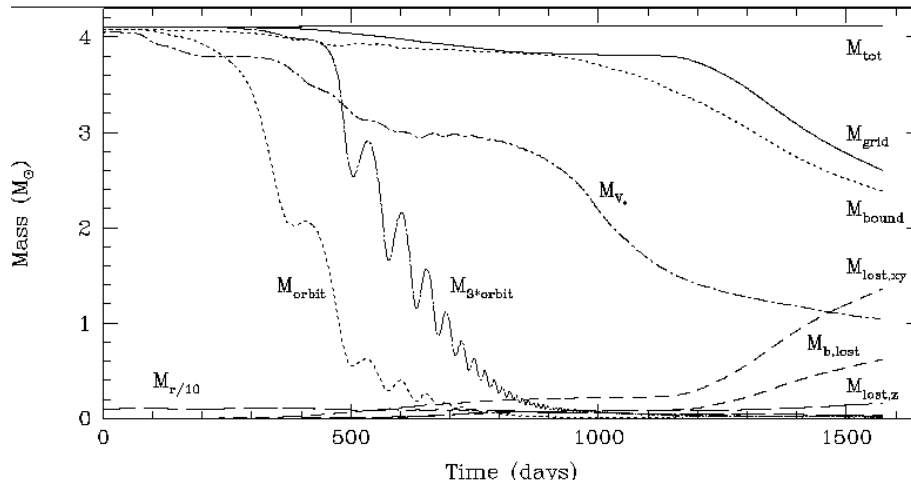


Fig. 15.— Tracers of gas mass for simulation 5. The curve labels have the same meaning as in Figure 8.

we find that the same *fraction* of the giant envelope is removed in half the time of the baseline simulation. At the end, the mass-loss timescale as judged from the bound mass is about 17 years and decreasing. However, most of this gas is marginally bound, and it is sufficiently far away that it does not influence the point-mass orbits in the short term. The mass in the original giant volume is decreasing considerably more quickly than in simulation 3.

#### 3.4.4. Sequence 5: evolved $5 M_{\odot}$ Giant, $0.6 M_{\odot}$ Companion, Nonsynchronous Rotation

As a test of the effects of the evolutionary state of the giant on the evolution, we conducted this simulation in which the  $5 M_{\odot}$  giant was in a more evolved state. The input giant model had a radius of  $2.46 \times 10^{13}$  cm, as opposed to  $1.32 \times 10^{13}$  cm for the previous runs with  $5 M_{\odot}$  giants. The carbon-oxygen (CO) core was  $0.87 M_{\odot}$ , and  $0.57 M_{\odot}$  for the previous runs. (The point mass had a slightly lower mass than for the previous runs because the point mass includes all the mass of the star up to the size scale of about the smallest zone. Even though the CO core is larger, the overall expansion of the giant, reduces the mass relegated to the point particle.) In addition, the orbit of the companion was moved out to a distance of  $3.7 \times 10^{13}$  cm.

The simulation was run for 1574 days, and the final separation of the point masses in this simulation was approximately twice that of the previous simulations. The mass tracers are shown in Figure 15. Because this could have been related to our numerical algorithm, we explored this possibility, as described in the next section. The result was that the smoothing length was found to affect the final separation, but not the efficiency of envelope ejection, which was found to remain roughly constant near 53%.

The spiral-in phase lasts for the first 300 days in this simulation, while the rapid infall phase



also lasts roughly twice as long as in the other simulations (ending at about 800 days). At the end, the mass loss timescale has increased to 16 years, while the orbital decay timescale is at 7 years, and both are increasing. The final outcome of the simulation will probably be ejection of the envelope since the gas within the giant’s volume is being pushed out quickly.

### 3.5. Numerical Effects

The later portions of the envelope ejection phase were not followed by Rasio & Livio (1996) because the local spatial resolution for their SPH gas particles near the cores was comparable to the size of the binary orbit. In our simulations, limitations on spatial resolution are present in the zone spacing on the grid the point masses occupy, and in the smoothing length applied to gravitational interactions between point masses and gas.

With regards to the effects of the smoothing length in the gas-to-point-mass potentials, the main questions are how critical the formulation of the potential is, and how physically realistic it is. The potential we have used crudely mimics the effects of constant density mass distributions in each gas zone, since the force due to a given zone is reduced when the point mass falls within the zone. The point masses are not strictly points, although their physical sizes (in the case of compact objects, including the cores of giant stars) are more than an order of magnitude smaller than the smoothing length. However, relatively small amounts of matter accreted onto these stars will cause the cores to partially fill their respective Roche or tidal lobes, creating configurations that are much larger (see Hjellming & Taam 1991) and comparable to the zone size. We expect that the smoothing length only becomes important towards the end of the simulations when the point mass orbits are small, meaning that the point masses orbit within and primarily interact with only a handful of zones.

To test the effects of the smoothing length, we allowed it to decrease once the point mass separation reached a distance of three times the smoothing length of one point mass. To an extent this is physically realistic if the “true” size of the point masses are on the order of the tidal radius, since the tidal radii will decrease as the orbital separation decreases. In making this change for the configuration of sequence 5, we find that the final orbital separation decreases from about  $8.9 R_{\odot}$  to  $5.3 R_{\odot}$ . We also ran the same simulations with a reduction in the number of subgrids from two to one to check the relative importance of the grid resolution itself. For a fixed potential smoothing length 1.5 times the smallest zone size (twice the size of sequence 4), we found the final separation was about  $16.9 R_{\odot}$ . When the smoothing length was fixed equal to the smallest zone size, the separation became about  $14.9 R_{\odot}$ . With the adjustable smoothing length algorithm, the final separation reached  $8.1 R_{\odot}$ .

For simulations with additional subgrids, we expect the computed final separations would converge on a value. However at our present level of resolution, we are unable to specify exactly how close our two point masses approach each other in the end. We should consider whether we

can put realistic limits on the final separation. It is safe to say that the separations derived from our fixed smoothing length simulations are good upper limits since higher resolution would tend to increase the amount of energy dissipation and angular momentum transfer. We applied the newer smoothing length algorithm to simulations 1, 3, and 4, and found that the final separation did decrease in all cases, but by no more than 25%. The additional energy input into the gas leads to the unbinding of considerably more mass and more mass loss off of the grid, while the amount of bound mass loss off the grid remains about the same. For simulation 3, the additional decrease in orbital separation and the resultant mass loss might be enough to eject the envelope.

The fact that the orbital separations still end up being nearly the same with the new smoothing length algorithm may indicate that the grid resolution has become the most important factor. We must conclude that it is unclear exactly how close the adjustable smoothing length algorithm brings us to the real physical separation.

There are a few final points we wish to make. First, the first two stages of the common envelope evolution are unaffected by this question, and most of the details of the envelope ejection phase will not change. For example, the efficiency of envelope ejection probably will not change much since the final separation is implicitly taken into account in the calculation. In fact, for several test versions we ran of sequence 5, the efficiency only varied by a few percent, despite differences in the final orbital separation and orbital energy of more than 50%. Second, in our simulations with fixed smoothing length, there is considerable eccentricity of the point mass orbits. This shows up in the rapid variations of the point-mass kinetic and core-companion gravitational energies in the late stages of the simulations. When we ran the same simulations with the smoothing length allowed to shrink with the orbit, the eccentricity is damped out. We believe this damping will be observed in higher resolution computations.

The anonymous referee points out that our conclusions about the degree of corotation of the gas immediately surrounding the two point masses may be affected by resolution effects. Rasio & Livio (1996) found that reducing the resolution (by reducing the number of particles) suppressed corotation of the gas at the end of the simulation. An examination of the present work and that of Rasio & Livio indicates that the two are not inconsistent with regards to the rotational state of gas farther from the cores. While the differences near the cores may be a function of numerical resolution, the results of the two studies indicate that the region of corotation is rather small in spatial extent (of the order of the binary separation) and negligible in mass, and hence dynamically unimportant.

### 3.6. Outcomes of Common Envelope Evolution

There are a number of physical effects that have not been included in our models of the common envelope evolution, but which may affect either our results, or our inferences about the eventual outcome of the interaction. In the following, we briefly discuss several.

As discussed in the previous section, we have modeled the core of the red giant and the companion star as point masses. As a result we neglect aerodynamic drag effects caused by the finite size of the stars and the gas they have accreted. This would only tend to influence the results during phases in which the density of gas impinging on the stars significantly affects the momentum of the stars. So, this probably does not affect the orbital evolution of the stars beyond the ends of our simulations, but could influence the rate at which the companion initially falls through the giant’s envelope, or the orbital decay before too much of the envelope is ejected from the vicinity of stars. Even so, for objects traveling at supersonic speeds through a gas, aerodynamic drag is found to be small in most cases compared to the gravitational drag (Kley, Shankar, & Burkert 1995), which we do model. Thus, we do not expect aerodynamic drag to play a large role.

It is also certain that radiation transfer becomes important at times beyond the end of the simulations. As the gas density of the nebula drops, the decrease in optical depth allows the gas to cool, removing internal energy that could have been used to unbind it. In addition, radiation from the white dwarf core of the red giant could help to power a wind that could assist in removing the remnants of the envelope. If gas is able to cool and contract back towards the cores, it could result in additional reduction of the core-companion separation. A rough calculation applying an analytic expression for bound-free opacities to the density and temperature distribution indicates that radiation diffusion timescales from the vicinity of the point masses are on the order of a thousand years at the end of the simulation. It seems clear that gas must rarefy considerably before radiation losses become important.

#### 4. Discussion

In this paper the hydrodynamical evolution of a binary system consisting of an AGB star and its main sequence companion has been followed from the initial to the late stages of the common envelope phase using high resolution numerical techniques. During the evolution, spiral density waves clearly show the coupling between the gas and the double core. The shrinkage of the companion orbit is very rapid, lasting only about 0.7 year. The orbital decay decelerates dramatically at an orbital separation of  $\lesssim 7R_\odot$ , although this may be due in part to the effects of finite spatial resolution. The double core is briefly embedded in a slowly expanding differentially-rotating pressure-supported disk, which remains loosely bound to the two cores. The matter within the original volume of the common envelope is spun up to only a fraction of corotation with the point masses, but energy input from the point mass orbits leads to mass removal at a rate of  $\sim 0.3 M_\odot \text{ yr}^{-1}$  at the end of the simulation.

The evolution to the late stages was followed for about an order of magnitude longer in time than Rasio & Livio’s (1996) SPH calculation. The results of our studies show that the late phases of the hydrodynamical evolution are not affected by the initial spiral-in of the companion into the giant star. That is, it is found that the degree to which the components are out of synchronous

rotation at the onset of the common envelope phase only affects the initial development. A slightly less rapid infall of the companion into the red giant envelope results. The final orbital separation of the remnant binary immediately following the ejection of the common envelope has not yet been reached in our simulations because of inadequate spatial resolution. For our first four simulations, a period of one day is found to be the upper limit. With a more evolved giant, the final period appears to increase.

The results of the numerical simulations suggest the successful ejection of the common envelope for a binary consisting of a  $3M_{\odot}$  giant with a  $0.7M_{\odot}$  core and a  $0.4M_{\odot}$  companion. On the other hand, the system may or may not merge for a higher mass giant of  $5M_{\odot}$  (with a  $1M_{\odot}$  core) with the same companion. The tendency toward merger for higher mass systems reflects the larger mass that must be ejected and the greater potential well from which the common envelope must escape. For more advanced stages in the evolution of the giant, a greater fraction of the mass is situated at larger distances from the degenerate core so that the energy requirements for ejection can be relaxed. However, the flat mass-radius profile extends to greater distances as well, implying that the final orbital separation will also be increased, so that less orbital energy may actually be available for ejecting the gas. Thus, successful envelope ejection for more evolved configurations is not as favorable as might be expected.

In all of our simulations the mass ejection is concentrated toward the equatorial plane with about five times as much mass loss in the orbital plane as compared to the polar direction. In addition, the results indicate that an expanding disk can form briefly about the remnant binary system. These morphologies may be consistent with the equatorial-to-polar density contrast required by the interacting winds model for the shaping of planetary nebulae. Specifically, the results described in Frank et al. (1993) and Mellema & Frank (1995) indicate that variations of three to five are adequate in providing an envelope morphology which resembles those planetary nebula systems exhibiting a clear axisymmetric structure. Furthermore, the presence of a geometrically thick disk may facilitate the formation of jets in planetary nebulae (Soker & Livio 1994).

The results obtained from these numerical simulations can be used to place constraints on the progenitor systems of planetary nebulae with binary nuclei, provided that orbital angular momentum losses from the remnant binary are insignificant following the common envelope phase. Angular momentum losses associated with either magnetic braking or gravitational radiation are unimportant for the binary stars within planetary nebulae since the age of the nebula (and hence the age of the post-common-envelope system) is characteristically less than about  $10^4$  years. Orbital evolution due to angular momentum transfer from the orbit to a circumbinary disk is also not expected to be significant since our results demonstrate that the majority of mass in the disk is situated at great distances (many times the orbital separation) from the binary system. Furthermore, the angular momentum loss from the orbit responsible for the spin-up and ejection of the remaining matter in the vicinity of the remnant binary ( $\lesssim 0.01M_{\odot}$ ) can be estimated from the study of Shu, Lubow, & Anderson (1979), and it is expected to reduce the orbital separation

only slightly (by about 10%).

The observational study of binary stars within planetary nebulae reveals that many systems (6 out of the 12 known, although this is affected by selection effects) have orbital periods less than 0.7 days (see Bond 1995). A total mass for the remnant binary of  $1 M_{\odot}$  implies that the orbital separation following the mass ejection phase of the common envelope is  $3.3R_{\odot}$ . Based on the present study and following the work of Terman & Taam (1996) on the estimated final orbital separations of post-common-envelope systems, it is found that white dwarf masses  $< 0.6M_{\odot}$  are indicated for systems with orbital periods less than 0.7 days. (For systems with orbital periods  $\gtrsim 0.7$  days, no such constraint can be placed on the white dwarf masses). It should be noted that white dwarf masses in the range from about 0.46 - 0.56  $M_{\odot}$  cannot be formed in the common envelope scenario since such core masses develop during the core helium burning phase of the red giant when the red giant is insufficiently large in radius to initiate mass transfer (see Webbink 1976). The progenitor masses leading to systems with orbital periods  $\lesssim 0.7$  days are less than  $3M_{\odot}$  as illustrated in Figure 16. Based on the present work, the final orbital separations have been estimated by assuming that they are a factor of 6 less than the radial distance in the giant corresponding to the point where the logarithmic derivative of the pressure with respect to radius is a minimum (this point marks the outer boundary of the flat portion of the flat mass-radius profile; see Terman & Taam 1996). Greater orbital separations correspond to progenitor stars in more advanced evolutionary phases with more massive cores. The result that lower white dwarf masses result from the lower mass range of intermediate mass stars is consistent with the seminal work of Paczynski (1970). The radii of these progenitor stars are  $\sim 10^{13}$  cm corresponding to orbital periods of the progenitor systems at the onset of the common envelope phase of  $\lesssim 0.5$  years.

To further our understanding of the outcome of the common envelope phase, higher resolution and longer term evolutionary studies will be necessary to follow the total ejection of the common envelope. Systematic studies will be required to determine the efficiency of mass ejection and to delineate the parameter space separating those systems which merge from those systems which survive the common envelope stage. Such studies will also illustrate the diversity of morphologies of ejected matter (formation of disks and density contrasts between the polar and equatorial directions) relevant to the shaping of planetary nebulae.

This work has been supported by NSF grant AST-9415423.

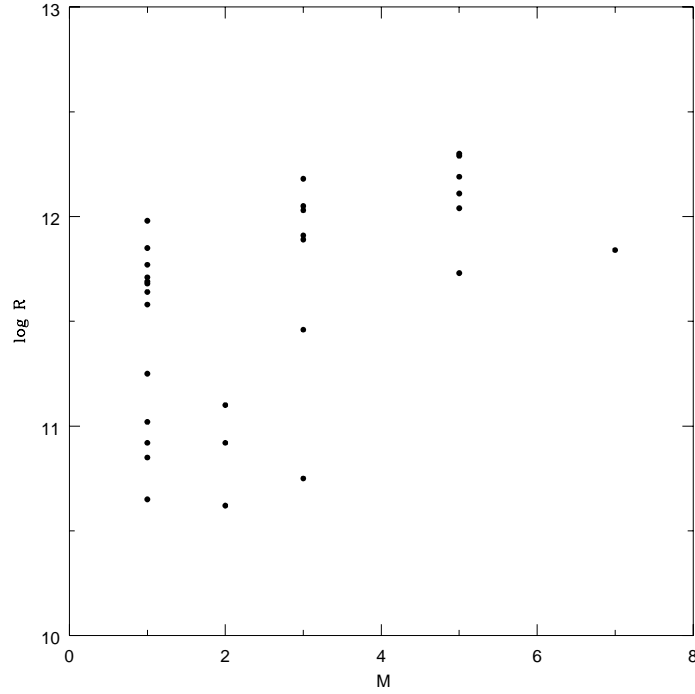


Fig. 16.— Orbital separation of a post-common-envelope binary system as a function of the red giant mass in solar units. The separation is assumed to be a factor of 6 less than the radius of the common envelope for which the logarithmic derivative of the pressure with respect to the radius is a minimum.

## REFERENCES

- Berger, M. J. & Colella, P. 1989, *J. Comp. Phys.*, 82, 64
- Berger, M. J. & Olinger, J. 1984, *J. Comp. Phys.*, 53, 484
- Bodenheimer, P. & Taam, R. E. 1984, *ApJ*, 280, 771
- Bond, H. E. 1995, in *Asymmetrical Planetary Nebulae*, ed. A. Harpaz & N. Soker (Bristol: Institute of Physics Publishing), 61
- Bond, H. E. & Livio, M. 1990, *ApJ*, 355, 568
- Burkert, A. & Bodenheimer, P. 1993, *MNRAS*, 264, 798
- Counselman, C. C. 1973, *ApJ*, 180, 307
- Darwin, G. H. 1879, *Proc. R. Soc. London*, 29, 168
- de Kool, M. 1987, Ph.D. Thesis, University of Amsterdam
- de Kool, M. 1992, *A&A*, 261, 188
- de Kool, M. 1996, in *Evolutionary Processes in Binary Stars*, ed. R. A. M. J. Wijers, M. B. Davies, & C. A. Tout, (Dordrecht: Kluwer), 365
- Delgado, A. J. 1980, *A&A*, 87, 343
- Eggleton, P. P. 1971, *MNRAS*, 151, 351
- Eggleton, P. P. 1972, *MNRAS*, 156, 361
- Frank, A., Balick, B., Icke, V., & Mellema, G. 1993, *ApJ*, 404, L25
- Gingold, R. A. & Monaghan, J. J. 1977, *MNRAS*, 181, 375
- Han, Z., Podsiadlowski, P., & Eggleton, P. P. 1995, *MNRAS*, 272, 800
- Hjellming, M. S. & Taam, R. E. 1991, *ApJ*, 370, 709
- Iben, I. & Livio, M. 1993, *PASP*, 105, 1373
- Iben, I. & Tutukov, A. V. 1984, *ApJS*, 54, 335
- Kalogera, V. & Webbink, R. F. 1996, *ApJ*, 458, 301
- Kley, W., Shankar, A., & Burkert, A. 1995, *A&A*, 297, 739
- Kopal, Z. 1978, *Dynamics of Close Binary Systems*, (Dordrecht: Reidel)
- Kwok, S. 1982, *ApJ*, 258, 280
- Lai, D., Rasio, F. A., & Shapiro, S. L. 1993, *ApJ*, 406, L63
- Lai, D., Rasio, F. A., & Shapiro, S. L. 1994, *ApJ*, 420, 811
- Livio, M. 1995, in *Asymmetrical Planetary Nebulae*, ed. A. Harpaz & N. Soker (Bristol: Institute of Physics Publishing), 51
- Livio, M. & Soker, N. 1984, *MNRAS*, 208, 763.

- Livio, M. & Soker, N. 1988, *ApJ*, 329, 764
- Lucy, L. 1977, *AJ*, 82, 1013
- Mellema, G. & Frank, A. 1995, in *Asymmetrical Planetary Nebulae*, ed. A. Harpaz & N. Soker (Bristol: Institute of Physics Publishing), 229
- Meyer, F. & Meyer-Hofmeister, E. 1979, *A&A*, 78, 179
- Monaghan, J. J. 1985, *Computer Physics Reports*, 3, 71
- Monaghan, J. J. 1992, *ARA&A*, 30, 543
- Paczynski, B. 1970, *Acta Astr.*, 20, 47
- Paczynski, B. 1976, in *IAU Symposium No. 73, The Structure and Evolution of Close Binary Systems*, ed. P. Eggleton, S. Mitton, & J. Whelan, (Dordrecht: Reidel), 75
- Paczynski, B. & Sienkiewicz, R. 1972, *Acta Astr.*, 22, 73
- Rasio, F. & Livio, M. 1996, *ApJ*, 471, 366
- Ruffert, M. 1993, *A&A*, 280, 141
- Shu, F. H., Lubow, S. H., & Anderson, L. 1979, *ApJ*, 229, 223
- Sod, G. A. 1978, *J. Comp. Phys.*, 27, 1
- Soker, N. & Livio, M. 1989, *ApJ*, 339, 268
- Soker, N. & Livio, M. 1994, *ApJ*, 421, 219
- Taam, R. E. & Bodenheimer, P. 1989, *ApJ*, 337, 849
- Taam, R. E. & Bodenheimer, P. 1991, *ApJ*, 373, 246
- Taam, R. E., Bodenheimer, P., & Ostriker, J. P. 1978, *ApJ*, 222, 269
- Terman, J. L. & Taam, R. E. 1996, *ApJ*, 458, 692
- Terman, J. L., Taam, R. E., & Hernquist, L. 1994, *ApJ*, 422, 729
- Terman, J. L., Taam, R. E., & Hernquist, L. 1995, *ApJ*, 445, 367
- Tutukov, A. V. & Yungelson, L. R. 1979, *Acta Astr.*, 29, 666
- van den Heuvel, E. P. J. 1987, in *High Energy Phenomena Around Collapsed Stars*, ed. F. Pacinin (Dordrecht: Reidel), 1
- van Leer, B. 1977, *J. Comp. Phys.*, 23, 276
- von Neumann, J. & Richtmeyer, R. D. 1950, *J. Appl. Phys.*, 21, 232
- Webbink, R. F. 1976, in *IAU Symposium No. 73, Structure and Evolution of Close Binary Systems*, ed. P. Eggleton, S. Mitton, & J. Whelan, (Dordrecht: Reidel), 207
- Webbink, R. F. 1979, in *IAU Coll. No. 46, Changing Trends in Variable Star Research*, ed. F. M. Bateson, J. Smak, & I. H. Urch (Hamilton, NZ: Univ. Waikato), 102
- Yorke, H. W., Bodenheimer, P., & Laughlin, G. 1993, *ApJ*, 411, 274



- Yorke, H. W., Bodenheimer, P. & Taam, R. E. 1995, ApJ, 451, 308
- Yungelson, L. R., Tutukov, A. V., & Livio, M. 1993, ApJ, 418, 794

Sequence	$M_1(\text{M}_\odot)$	$M_c(\text{M}_\odot)$	$M_2(\text{M}_\odot)$	$f_{sync}$
1	3	0.7	0.4	1.0
2	3	0.7	0.4	0.0
3	5	1.0	0.4	1.0
4	5	1.0	0.6	1.0
5	5	0.94	0.6	0.0

Table 1: Initial Parameters of Common Envelope Sequences

Sequence	$a(\text{R}_\odot)$	$P$ (days)	$v$ ( $\text{km s}^{-1}$ )	$\alpha_{CE}$
1	4.42	1.03	3	0.38
2	4.68	1.12	4	0.46
3	4.37	0.90	4	0.24
4	4.78	0.96	1	0.44
5	8.91	2.48	2	0.53

Table 2: Final Parameters of Common Envelope Sequences